J Appl Electrochem (2011) 41:1033–1042
DOI 10.1007/s10800-011-0341-9

ORIGINAL PAPER

# Characterisation of a electrochemical hydrogen pump using electrochemical impedance spectroscopy

**M.-T. Nguyen · S. A. Grigoriev · A. A. Kalinnikov · A. A. Filippov · P. Millet · V. N. Fateev**

Received: 17 December 2010 / Accepted: 16 July 2011 / Published online: 23 August 2011


**Abstract** Electrochemical hydrogen pumps are electrochemical devices which are used for hydrogen purification and pressurization purposes. In such cells, gaseous hydrogen is oxidized at the anode and released at the cathode. Results presented in this paper are related to the characterization and optimization of a proton-exchange membrane (PEM) hydrogen pump using electrochemical impedance spectroscopy (EIS). Only the case of hydrogen purification is considered here. Current–voltage characteristics have been measured. The kinetics and efficiency of the cell have been investigated using EIS. The roles played by the cell structure (in particular by the ion-exchange polymer content in the electro-catalytic layers) and by different operating parameters (the cell temperature, the relative humidity and the partial pressure of hydrogen) on the overall process efficiency have been evaluated and are discussed.

M.-T. Nguyen · P. Millet
Institut de Chimie Moléculaire et des Matériaux,
UMR CNRS no. 8182, Université Paris Sud, bât 420,
91405 Orsay Cedex, France

S. A. Grigoriev (✉) · A. A. Kalinnikov ·
A. A. Filippov · V. N. Fateev
Hydrogen Energy and Plasma Technology Institute,
National Research Center "Kurchatov Institute",
Kurchatov sq., 1, Moscow, Russia 123182
e-mail: s.grigoriev@hepti.kiae.ru

S. A. Grigoriev
International Institute for Applied Physics and High
Technologies, Raspletina str., 4/1, Moscow, Russia 123060

A. A. Kalinnikov
LLC "Fast Engineering M", Novocheryemushkinskaya str.,
21-1-191, Moscow, Russia 117218

**Keywords** Proton-exchange membrane (PEM) · Hydrogen pump · Hydrogen purification · Hydrogen compression · Impedance spectroscopy · Optimisation

## 1 Introduction

With an annual consumption rate of nearly 650 billion $Nm^3$/year, hydrogen is widely used as a raw material in the chemical industry. Currently, the dominant technology used for its direct production is the steam reforming of natural hydrocarbons such as natural gas. Over the last decades, hydrogen has also been considered as a potential energy carrier which could be used for the promotion of renewable energy sources and the replacement of natural hydro-carbonated fuels. In this general context, many industrial processes require purified and pressurized hydrogen. Electricity-assisted hydrogen extraction from miscellaneous gas mixtures and compression in order to meet the requirements of various downstream processes is therefore of great practical interest. According to the electrochemical literature, hydrogen purification and compression can be achieved using a two-step process: (i) a first electrochemical cell can be used for the purpose of purifying/concentrating hydrogen from raw industrial sources; (ii) a second electrochemical cell can be used to pressurize the purified hydrogen. However, it is also possible to combine both concentration and pressurisation steps using one single cell in order to produce pure and pressurized hydrogen from raw industrial gas mixtures [1]. Proton-Exchange Membrane (PEM) technology is frequently mentioned as an interesting technology for that purpose because PEM cells offer some significant advantages: because of the high selectivity of the electrochemical process and the reasonably low permeability of the solid

polymer electrolyte, pure (up to 99.99 vol.%) and pressurized (at pressures up to 50 bar and even more by connecting several compression units in series) hydrogen can be obtained. Also, due to the thin membrane-electrode assemblies (MEAs) used in PEM technology (less than 1 mm), a limited energy consumption of approximately 0.6 $kWh/Nm^3$ hydrogen (total power costs for separation and compression) is required [1]. In terms of applications, it is expected that hydrogen concentration and compression based on this technology will find applications in various industrial fields such as (i) separation and recycling of hydrogen used as cooling agent in turbines; (ii) separation of hydrogen from products of organic fuel conversion [2]; (iii) separation of hydrogen from waste gases of fuel cells; (iv) concentration and separation of hydrogen isotopes (cooling of nuclear reactors) [3, 4]; (v) separation of hydrogen from mixtures with natural gas (so-called, "hythane"), in particular, after transportation of hythane through gas pipelines [5].

The main characteristics of PEM purification/compression cells have been described in a previous paper [1]. In the present study, we report on results related to the optimisation of electrode microstructure and to the critical issue of water management in such cells, using electrochemical impedance spectroscopy (EIS) as investigation tool. Only the case of hydrogen purification is considered here. Most results pertain to the case where pure hydrogen is used but mass transport limitations arising from the use of diluted hydrogen are also considered to a lesser extend. As for any other electrochemical process, the efficiency of the electrochemical purification step depends largely on the activity of the two electrodes [6]: the anode where the gas-phase hydrogen oxidation reaction (HOR) and the cathode where the hydrogen evolution reaction (HER) are respectively taking place. Carbon-supported platinum particles are known to be the most efficient catalysts for these reactions. However, catalysts must be coated onto the solid polymer electrolyte (SPE) in such a way that a maximum number of catalyst particles are made available for the electrochemical charge-transfer reactions. To some extent, the internal resistance of the MEA can therefore be adjusted by monitoring the amount of the ion-exchange polymer in the catalytic layers. We report on such issues and provide data on the most suited electrode composition. In terms of operating conditions, both the ohmic resistance of the ion-conducting polymer membrane and the catalytic activity of the MEAs are temperature-dependent. Appropriate operating conditions therefore play a significant role on the overall efficiency of the process. In conventional PEM technology, perfluorinated sulfonic acid polymer materials are used as SPE. The temperature domain of operation ranges from sub-zero up to a maximum value close to 100 °C (at higher operating temperatures, water swelling become so important that membranes loose their mechanical properties and rapidly fall apart). A temperature close to 90 °C can be considered as an optimum at which the energy efficiency is maximized. Besides the temperature of operation, the water content of the SPE is another critical parameter. The membrane must be adequately humidified to minimize its resistivity and to avoid electrode flooding and related mass transport limitations which can significantly reduce the efficiency of the process. From a practical viewpoint, water management issues were treated by adding a gas humidifier in the feed line to the most sensitive electrode of the PEM cell (the anode where the HOR is taking place) and by monitoring the temperature of the PEM cell. The humidifier was used to set the water vapour content of the hydrogen source and the temperature of the cell was set to such values that risks of water condensation and electrode flooding were prevented.

## 2 Experimental section

### 2.1 Description of the MEA

Basic principles of hydrogen compression/concentration PEM cells can be found in Refs. [1, 7]. Hydrogen purification is an electron-driven process ($\Delta G > 0$). Hydrogen is oxidized into protons at the anode, protons migrate across the cell according to the electric field and molecular hydrogen is evolved at the cathode. This is a highly efficient Faradic process which can potentially be used to extract and concentrate hydrogen from miscellaneous gas mixtures and produce purified hydrogen. Furthermore, it is possible to pressurize the cathodic compartment in order to increase delivery pressure. As a result, hydrogen is transferred from the low pressure (LP) anodic compartment to the high pressure (HP) cathodic compartment. Several tens of bars can be reached in a single step using single cells. Thus, purification and compression steps are combined in one single step. Electrochemical reactions taking place in the process at the electrode–solid polymer electrolyte (SPE) interfaces are those of Eqs. 1 and 2. Equation 3 is the overall cell reaction:

$$\text{anode: } H_2(LP) \rightarrow 2H^+ + 2e^- \quad (1)$$

$$\text{cathode: } 2H^+ + 2e^- \rightarrow H_2(HP) \quad (2)$$

$$\text{overall reaction: } H_2(LP) \rightarrow H_2(HP) \quad (3)$$

The extent to which hydrogen can be purified and compressed using PEM technology depends mostly on the characteristics of the solid polymer electrolyte (SPE) used in the cell. As in PEM fuel cell and water electrolysis technologies, SPE used in compression/purification PEM cells are made of perfluorosulfonic proton-conducting

materials. Gas solubility in such materials is relatively low but still sufficient to let significant permeation flows to occur when a gradient of chemical potential is set across the membrane. Gas transfer from one compartment of the cell to the other is a diffusion-driven process. This is why gas permeation flows are proportional to the gradient of pressure. As a result, gas purity and Faradic efficiency of the compression process tend to decrease when operating pressure is raised. In spite of these limitations, electrochemical purification/compression offers some interesting features. This type of system has no moving part and is very compact. MEAs can be stacked to form multi-stage compression units. Pressure of several hundred bars can potentially be reached. The partial pressure of water vapor in the feed gas, current density, operating temperature and hydrogen back diffusion due to the pressure gradient are the main parameters affecting the maximum output pressure and the overall efficiency of the process.

Assuming that hydrogen behaves as an ideal gas (an assumption which is reasonably acceptable up to pressures of several bars), the thermodynamic voltage of the compression process can be approached by the ratio of input and output pressures. A quantitative expression can be readily derived from the Nernst equation:

$$E\,(V) \;=\; \frac{RT}{2F}\; Ln\; \frac{P_{H_2}^{HP}}{P_{H_2}^{LP}} \tag{4}$$

When the cell is used only for hydrogen purification purposes (and not for compression), $\Delta P = P_{H_2}^{HP} - P_{H_2}^{LP} = 0$ bar and, according to Eq. 4, $E = 0$ V. When the cell is used for pressurizing hydrogen, a thermodynamic cell voltage of 30 mV is required at 298 K for a tenfold compression factor. Would reactions (1) and (2) take place at low current density (close to the thermodynamic voltage), no electric power would be needed. In practical cases however, high current densities are targeted to reduce investment costs and electric power is required to overcome overvoltages associated with reactions (1) and (2) as well as the resistivity of the SPE. However, the kinetics of interfacial charge transfer processes at platinum–SPE interfaces is known to be high and therefore, the electric power consumption should be limited to the ohmic drop across the SPE during operation. Experiments reported in this paper were obtained using 7 $cm^2$ MEAs. A lab-made electrocatalyst containing 40 wt% platinum deposited on a Vulcan XC-72 (Cabot company) carbon carrier of large (250 $m^2\ g^{-1}$) specific area and referred to as Pt40/Vulcan XC-72 [8] was used at both anode and cathode. In most experiments, the noble metal content was 1.0 mg/$cm^2$ at the cathode and 0.7 mg/$cm^2$ at the anode. The carbon supported catalyst was then dissolved in isopropanol. A solution of perfluorosulfonic acid ionomer in isopropanol was added under continuous and vigorous stirring. The polymer content at the anode was set to 15 wt. % and the polymer content at the cathode was adjusted in the 5–25 wt. % range. Catalytic inks thus obtained were then sprayed directly onto the surface of the Nafion-117 SPE. Sigracet 10 bb (SGL Carbon Group) carbon paper was used as anode gas diffusion layers. Porous titanium discs [9] with porosity of ca. 30% were used as current collectors at the cathode.

### 2.2 Description of the compression cell

The cell used for the measurements has been described elsewhere [1]. Briefly, the membrane–electrode assembly (MEA) of circular shape (7 $cm^2$) is clamped between two current collectors. The anodic current collector is made of hydrophobic porous carbon material (as in PEM fuel cells), and the cathodic current collector is a porous titanium sheet (commonly used in PEM water electrolysis technology [10]). Two gaskets made of fluorine rubber are used to prevent gas leakage during operation. Current collectors are pressed against the membrane using two external titanium flanges. Millimeter-thick grooves were machine made in the flanges to manage a space for hydrogen admission at the anode and to collect hydrogen–water mixtures at the cathode. The cell was tight using stainless steel nuts and bolts. Nuts were covered with an insulating layer of silicon to avoid electrical short-circuits. Polarisation curves and impedance diagrams were recorded using a Solartron 1285 potentiostat/galvanostat. Only the global cell impedances were measured, not individual electrode impedances.

### 2.3 Relative humidity of hydrogen

As in fuel cells [11–13], the relative humidity of the hydrogen gas supplied to the anode plays a critical role. A laboratory gas humidifier was used to set the relative humidity of the hydrogen gas. The humidifier was placed between the hydrogen source (a PEM water electrolyzer) and the measurement cell. The humidifier was operated as follows. First, liquid water in the humidifier, the hydrogen admission line to the measurement cell and the anodic cell compartment were air-purged by continuous circulation of dry hydrogen. The water vapor content of the hydrogen-water gas mixtures entering the measurement cell was not directly measured. However, it was possible to adjust the partial pressure of water vapor in hydrogen (and therefore the relative humidity) by setting the temperature of the humidifier. The hydrogen flow across the gas humidifier was sufficiently low to reach equilibrium. Therefore the water vapor concentration in hydrogen is assumed to be

close to the saturation partial pressure at the temperature of operation of the humidifier.

## 3 Results and discussion

### 3.1 Polarisation curves

In a first set of experiments, polarization curves were recorded under various operating conditions. It rapidly turned-out that, for a given MEA, hydrogen humidification on the anodic side of the measurement cell was playing a critical role in the overall process efficiency. This is due to the fact that protons transferred across the solid polymer electrolyte during operation require hydration water molecules (electro-osmotic drag), a process also encountered in PEM fuel cells and in PEM water electrolysis cells. If water management issues are not properly managed, two limiting cases are observed: (i) when hydrogen supplied to the anode is not sufficiently hydrated, water depletion occurs and the resistivity of the membrane increases (at least in the vicinity of the anode); (ii) when the amount of water supplied to the anode is too important, water flooding occurs (causing mass transport limitations). To avoid such critical problems, it is necessary to manage hydrogen-hydration issues properly. For this purpose, a gas humidifier has been used on the anodic side (see experimental section) and both the temperature of the gas humidifier ($T_{hum}$) and the temperature of the measurement cell ($T_{cell}$) have been used as main experimental parameters. The sensitivity of the PEM cell to operating temperature is such that only minor temperature changes can lead to significantly different electrochemical performances. Some typical results (obtained at atmospheric pressure) using a MEA containing 25 wt. % of polymer at the cathode are plotted in Fig. 1 (values are corrected for the electronic impedance of the measurement titanium cell). As discussed above, the thermodynamic voltage at atmospheric pressure is zero but a significant voltage up to 1 volt (Fig. 1) is required experimentally to obtain a current density of practical interest (in the A $cm^{-2}$ range). Irreversibilities are due to electrode charge transfer overvoltages (hydrogen oxidation at the anode and proton reduction at the cathode) and to the ohmic drop across the solid polymer electrolyte membrane. The shapes of the different polarisation curves are similar to those measured on PEM fuel cell [14]. This is not surprising and very typical of the presence of at least one gas-consuming electrode in the cell (hydrogen oxidation at the anode in the present case). At low current densities, polarisation curves are logically logarithmic in shape, suggesting that charge transfer processes at one or both electrodes are rate-determining. In the intermediate current density range, a linear relationship is observed and this can

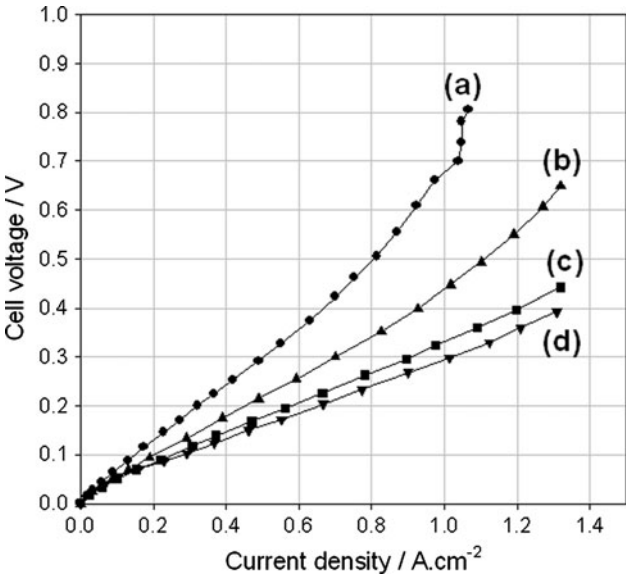


**Fig. 1** Current-voltage characteristics measured under various operating temperature modes. (*a*) $T_{hum} = 30$ °C; $T_{cell} = 23$ °C; (*b*) $T_{hum} = 45$ °C; $T_{cell} = 40$ °C; (*c*) $T_{hum} = T_{cell} = 60$ °C; (*d*) $T_{hum} = T_{cell} = 69$ °C

be attributed to ohmic drop limitations inside the polymer electrolyte. At high current density values, there is a tendency to reach a limiting current value. This appears clearly for the two less efficient curves at 23 and 40 °C and less clearly the two more efficient curves at 60 and 69 °C (nevertheless an inflexion point is still observed at 1.2 A $cm^{-2}$ indicating a change in the kinetics). As for fuel cells, a simple interpretation for this current limitation is that mass transport phenomena are taking place. Since here there is only one gas-electrode, the limitations can be attributed to the anode where gaseous hydrogen is oxidized into protons. This can be due to electrode flooding (inadequate water content in the feed gas and water condensation) or to the transport of gaseous hydrogen to the reaction sites at such high current densities. From Fig. 1, it appears that, when $T_{hum} > T_{cell}$, there is a tendency to electrode flooding and mass transport limitations. The best performances were obtained when the cell and humidifier temperatures had close values ($T_{hum} \approx T_{cell} \approx 70$ °C). Under such conditions, anode flooding could be avoided and a sufficient amount of water could be supplied to the membrane for humidification purpose. When $T_{hum} < T_{cell}$ (a case not represented in Fig. 1) the membrane is not adequately humidified and there is a tendency to higher ohmic resistance. From these different measurements and general observations, it can be concluded that improved electrochemical performances could be obtained by optimizing the structure of the MEAs and by meticulously controlling the water content of hydrogen (in order to balance the hydrogen flow and the humidification level). Results are reported in the next subsections.

### 3.2 Membrane resistance

Tests were carried out using electrochemical impedance spectroscopy (EIS) to evaluate the conductivity of the MEA and the efficiency of the catalytic layers as a function of water content in the feed hydrogen (water content was set by monitoring separately the temperatures of the humidifier and the measurement cell, as indicated above). In the followings, the expression "temperature mode" is making reference to a set of experimental conditions in which both the humidifier and measurement cell temperatures are set to particular values. Impedance diagrams measured at $E = 0$ Volt for three different temperature modes are plotted in Fig. 2 (impedance values are corrected for the electronic impedance of the measurement cell). Two more or less separated semi-circles are observed along the real axis. Considering that only one–electron charge transfer processes are taking place at each of the two electrodes (the HOR at the anode and the HER at the cathode), each semi-circle can be attributed to each electrode. The resistance of the solid polymer electrolyte is given by the high frequency intercept of the impedance diagrams with the real axis. At 0 V, there is no stationary charge transfer process. However, the PEM cell cannot be seen as the series connection of two capacitances. The amplitude (±10 mV) of the ac sine potential perturbation used for the measurements is sufficient to let a Faradic current flow through the cell and, as a result, the low frequency impedance is real. However, as can be seen from Fig. 2, impedance diagrams are significantly different for the three temperature modes under consideration. The ohmic resistance is minimized at optimal operating condition ($T_{cell} = 70$ °C; $T_{hum} = 65$ °C).

According to the literature, the resistivity $\rho_m$ of the solid polymer electrolyte (reverse value of the membrane conductivity $\sigma_m$) can be approximated (in the limited 288–373 K temperature range of investigation considered here) by [15]:

$$\rho_m = \frac{1}{\sigma_m} = \rho_m^{293\,K} \frac{T}{6,815 \cdot T - 1703,75}$$

where $\rho_m^{293\ K}$ is the specific resistance of the membrane saturated with water at 293 K. In the temperature range investigated here, the resistance of the membrane is approximately:

$$R_m\ (288\ K) = 0.21\,\Omega\,cm^2$$

$$R_m\ (373\ K) = 0.11\,\Omega\,cm^2$$

Experimentally, it is observed that there is a tendency for the membrane resistance $R_m$ (the high frequency limit of the impedance diagrams) to decrease with increasing relative humidity and to increase with operating current density (values measured for different cell temperatures are plotted in Fig. 3).

This is due to the transport of water with solvated protons from the anode to the cathode where liquid water is released. As the current density increases, the membrane becomes less hydrated and its resistivity increases. Best

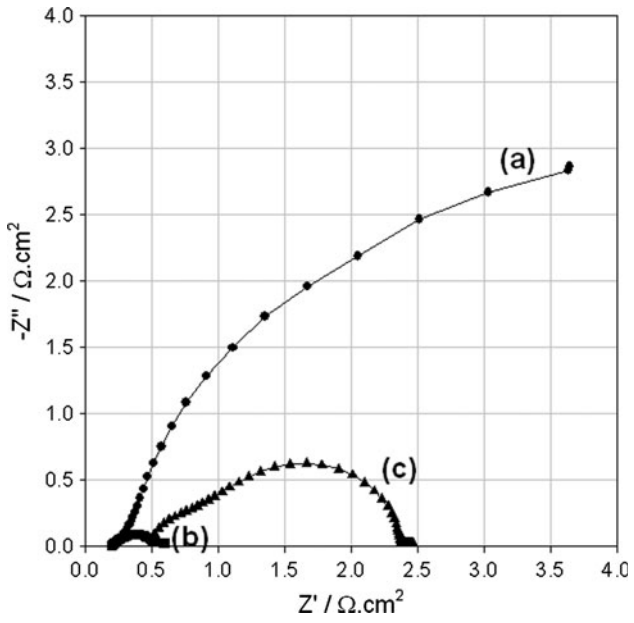


**Fig. 2** Impedance diagrams measured at $E = 0$ V ($i = 0$ A.cm$^{-2}$) for three different temperature modes: (*a*) $T_{hum} = 55$ °C; $T_{cell} = 60$ °C; (*b*) $T_{hum} = 65$ °C; $T_{cell} = 70$ °C; (*c*) $T_{hum} = 65$ °C; $T_{cell} = 78$ °C

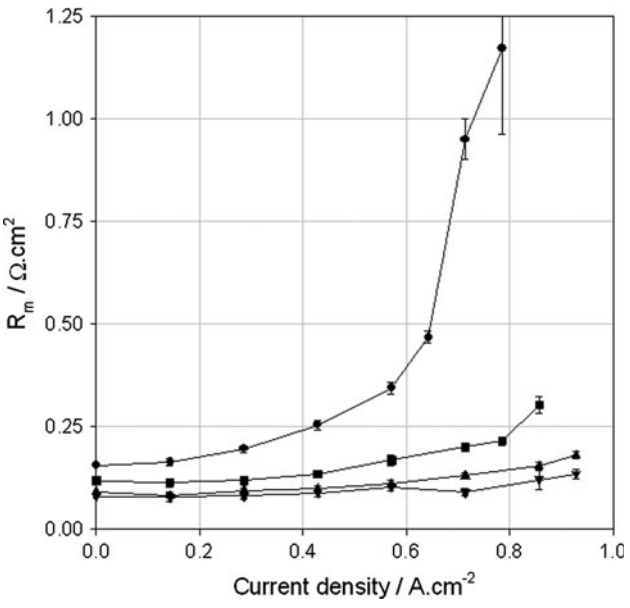


**Fig. 3** Absolute electrolyte resistance measured as a function of current density at different temperatures of the gas humidifier: (*filled circle*) 23 °C; (*filled square*) 39 °C; (*filled triangle*) 60 °C; (*filled inverted triangle*) 70 °C. $T_{cell} = 70$ °C

results are obtained when the temperature of the gas humidifier is higher than 65 °C (an optimum was found at ≈70 °C) and when the cell temperature equals that of the humidifier temperature.

### 3.3 Efficiency of the catalytic layers

Then, the effect of $T_{hum}$ and $T_{cell}$ on the global cell impedance was investigated. Setting the temperature of the gas humidifier to 65 °C and the temperature of the measurement cell to 70 °C (i.e. the case where $T_{cell} > T_{hum}$ to avoid water flooding), impedance diagrams have been measured at two different cell voltages (Fig. 4). Impedance values are corrected for the electronic impedance of the measurement cell. The high frequency limit of the cell impedance is the same in both cases (this is the ionic resistance of the membrane). The diameter of the two semi-circles (which are not fully separated) decreases when the cell voltage increases. At such low cell voltage values, charge transfer processes at electrodes are rate-determining (see Fig. 1) and the associated charge transfer resistance logically decrease with electrode potentials (Butler–Volmer). When the cell voltage is set to a constant value and when only the temperature modes differ (in Fig. 5 where impedance values are corrected for the electronic impedance of the measurement cell, $T_{cell} > T_{hum}$ to avoid flooding in both experiments), then the impedance diagram is shifted along the real axis toward the origin (less resistive values) because the resistance of the membrane decreases when the temperature increases.

Three different impedance diagrams measured at the same cell voltage (0.1 V) but for three different temperature modes are plotted in Fig. 6 (impedance values are corrected for the electronic impedance of the measurement cell).

Plots (a) and (b) are those of Fig. 5. Plot (c) was obtained for $T_{cell} = 78$ °C and $T_{hum} = 65$ °C. Such temperature conditions should be favourable since $T_{cell} > T_{hum}$ and in this case, electrode flooding is prevented. However,

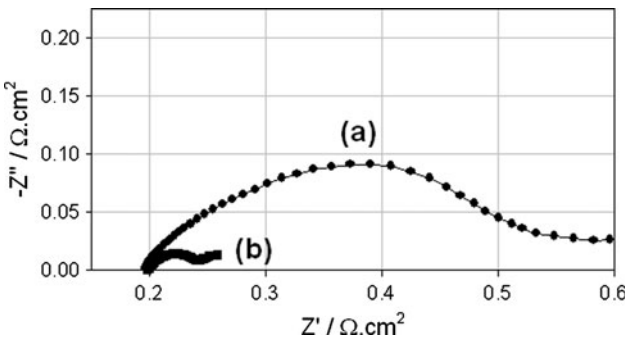


**Fig. 4** MEA impedance diagrams measured at $T_{hum} = 65$ °C and $T_{cell} = 70$ °C) for two different cell voltages: (*a*) 0 V; (*b*) 0.1 V

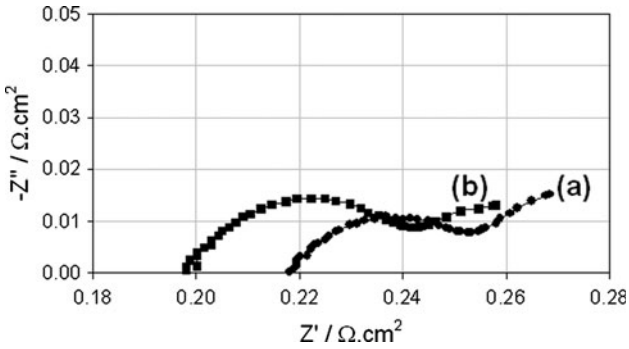


**Fig. 5** Impedance diagrams measured at 0.1 V for two different temperatures modes: (*a*) $T_{hum} = 55$ °C; $T_{cell} = 60$ °C. (*b*) $T_{hum} = 65$ °C; $T_{cell} = 70$ °C

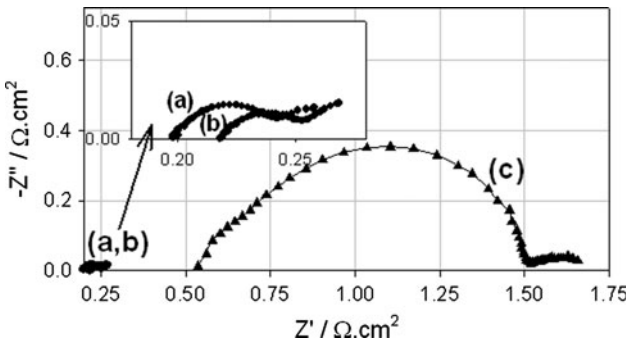


**Fig. 6** Impedance spectrums for three temperature modes (cell voltage = 100 mV): (*a*) $T_{hum} = 55$ °C; $T_{cell} = 60$ °C. (*b*) $T_{hum} = 65$ °C; $T_{cell} = 70°$. (*c*) $T_{hum} = 65$ °C; $T_{cell} = 78$ °C

the difference $T_{cell} - T_{hum} = 13$ °C is large. According to Fig. 1, a stationary current density of ≈200 mA $cm^{-2}$ is obtained at such cell voltage (0.1 V) and hydrogen supplied to the anode of the measurement cell is insufficiently hydrated to provide water molecules for each proton formed at the anode. As a result, the resistance of the membrane significantly increases (local drying) and the high resistance value of the impedance is shifted along the real axis to high resistance values. Also, the diameter of the first semi-circle (which can thus be attributed to the HOR at the anode) increases significantly. This is an indication that the kinetics of the charge transfer process at the anode is also impacted by the lack of water.

### 3.4 Optimisation of electrode structure

The ohmic resistance of the solid polymer membrane is expected to play a negligible role at low current densities. Therefore, the increasing current density with cell voltage observed in Fig. 1 at low current density values is mostly due to charge transfer kinetics at any or both electrodes. The exponential relationship between current and cell potential supports this viewpoint. To improve cell efficiency and reduce cell overvoltages at any given current

density value, it is necessary to choose efficient electrocatalysts (by selecting those offering the larger exchange current density value for the reaction of interest) or to increase as much as possible the roughness factor of the electrodes, and preferably to do both. Platinum is known to be the most efficient electrocatalyst for both the HOR and HER. Optimized carbon—supported platinum nanoparticles have become commercially available. They have high catalytic activity and the noble metal content is minimized to meet cost requirements in PEM fuel cell technology. To take full advantage of such catalysts, it is however necessary to improve the microstructure of the catalytic layers in order to obtain a high concentration of so-called 3D contact points, i.e. regions where the electron conducting phase (supported catalyst), the ion-conducting phase (polymer) and the gas phase (hydrogen) are in a sufficiently close vicinity to avoid that a substantial part of the catalyst particles remain inactive during cell operation. This issue is particularly critical at gas electrodes such as the anode of the concentration/compression PEM cells considered here. Therefore, in order to improve the cell efficiency, we tried to optimize the only parameter that was left, namely the polymer content of the electrodes, in order to avoid as much as possible idle catalyst particles. Different MEAs having a constant polymer content at the anode (15 wt. %) but different polymer contents at the cathode (from 5 up to 25 wt. %) have been prepared and tested. The polymer content is expected to play a role on the electrochemical performances of the cell because it is involved in both the conductivity and activity of the catalytic layer. Impedance spectra measured on a cell with a high (25 wt. %) and a low (5 wt. %) polymer content at the cathode for different operating temperatures and different cell voltages are plotted in Fig. 7 (impedance values are corrected for the electronic impedance of the measurement cell).

The purpose of Fig. 7 is not only to compare the high frequency limit of the impedance (due to the membrane resistance) but also the low frequency limit (which includes charge transfer overvoltages and therefore electrode structure with different polymer contents). The lowest overall MEA resistance value was obtained when the cell temperature was equal to the humidifier temperature (70 °C). Figure 7 also shows that, when the cell operates at the optimum temperature (≈70 °C), the MEA with the larger polymer content (25 wt. %) at the cathode offers the lowest overall resistance. With a polymer content of 25%, the activity of the catalyst layer is therefore higher than when the polymer content is only 5% (the diameter of the semi-circle along the real axis is smaller). It can therefore be concluded that the polymer content in the catalytic layer plays a significant role in the sense that its concentration is directly related to the amount of catalyst particles which are involved in the charge transfer processes at electrode–electrolyte interfaces.

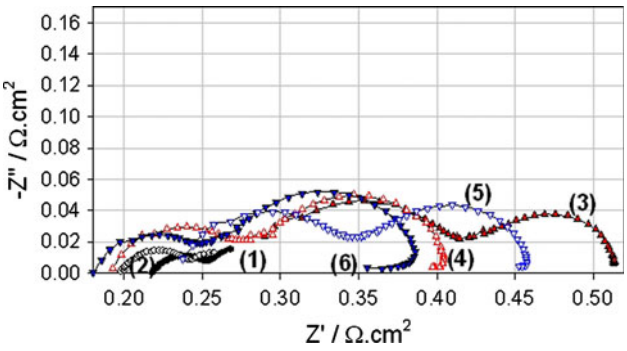


**Fig. 7** Impedance spectrums recorded at various operating temperatures using MEAs with different polymer contents (measurement cell impedance corrected): (*1*): 25wt.%; $T_{cell} = 69$ °C; $T_{hum} = 69$ °C; $U_{cell} = 0.075$ V. (*2*): 25wt.%; $T_{cell} = 60$ °C; $T_{hum} = 60$ °C; $U_{cell} = 0.075$ V. (*3*): 25wt.%; $T_{cell} = 40$ °C; $T_{hum} = 40$ °C; $U_{cell} = 0.1$ V. (*4*): 25wt.%; $T_{cell} = 25$ °C; $T_{hum} = 25$ °C; $U_{cell} = 0.15$ V. (*5*): 5wt.%; $T_{cell} = 70$ °C; $T_{hum} = 65$ °C; $U_{cell} = 0.1$ V. (*6*): 5wt.%; $T_{cell} = 60$ °C; $T_{hum} = 55$ °C; $U_{cell} = 0.1$ V

### 3.5 Water management issues

As discussed in the previous sections, if water management issues are not properly handled, liquid water forms at the anode and mass transport of dissolved hydrogen becomes the rate-determining step of the overall process. This effect is due of water flooding effects. It can be more or less significant. In some cases (when $T_{hum} \gg T_{cell}$), water condensation in the cell is such that hydrogen transport to the reaction sites is extremely limited. As a result, very small limiting current densities (a few mA $cm^{-2}$) are obtained. An example is provided in Fig. 8.

The shape of the impedance diagrams measured in such conditions differs from those obtained when there is no electrode flooding (Fig. 9: impedance values are not corrected for the electronic impedance of the measurement cell). In particular, the low frequency impedance values are not real. There is a tendency to form characteristic low frequency 45° semi-lines. This is an indication that diffusion-controlled processes become rate-determining. It is doubtful that hydrogen transport away from the cathode can have such a high impact on the overall cell impedance. Most probably, hydrogen dissolution in liquid water and transport up to the anode is responsible for this behaviour. The situation is reversible. When flooding conditions are met, the anode can be dried by a flow of dry and inert gas such as argon. The electrochemical performances obtained after this treatment are then close to those plotted in Fig. 1.

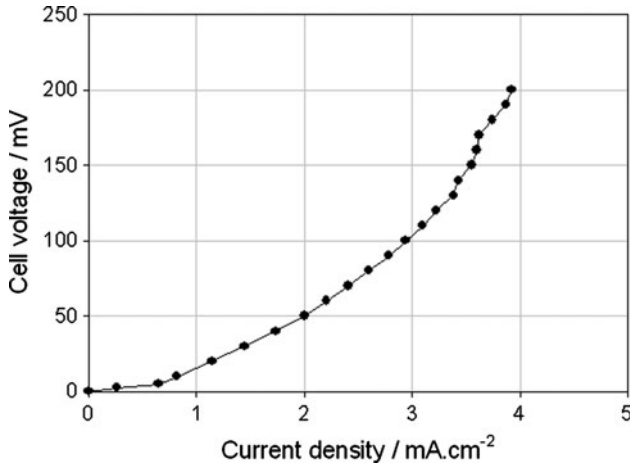


**Fig. 8** Current-voltage characteristics recorded under flooding conditions: $T_{hum} = 70$ °C; $T_{cell} = 40$ °C

### 3.6 Effect of hydrogen partial pressure

Additional experiments have been made to determine the effect of hydrogen partial pressure on cell characteristics at constant operating conditions. Hydrogen—argon gas mixtures have been used for that purpose. The water vapor concentration of the gas mixture is assumed to be close to the saturation partial pressure at the temperature of operation of the humidifier. To facilitate the interpretation of the data, a MEA containing an increased noble metal content of 2.0 mg/cm$^2$ at the cathode and only 0.5 mg/cm$^2$ at the anode has been prepared. Typical polarization curves recorded for three different $H_2$/Ar mole ratios are plotted in Fig. 10 (values are not corrected for the electronic impedance of the measurement cell; hence, performances are lower than those plotted in Fig. 1). The slope of the polarization curve significantly increases as the hydrogen content of the feed mixture decreases. For $H_2$/Ar = 0.3, a very small current density of 1 mA cm$^{-2}$ was measured.

AC impedance measurements have been performed for the three $H_2$/Ar compositions at a constant cell voltage of $E = 0.1$ V and constant temperature. Results are plotted in Fig. 11 (impedance values are not corrected for the electronic impedance of the measurement cell). The slope of the polarization curves in Fig. 10 is a measure of the cell impedance in stationary conditions (at very low frequency). For consistency, it can be observed that the low-frequency limits of curves (a) and (b) on the real axis (Fig. 11) are similar to the slope of the corresponding curves in Fig. 10. In Fig. 11, only one semi-circle is obtained. This is an indication that the cell impedance is mostly due to the contribution of the anode and that the kinetics of the HER is fast (as mentioned above, the catalyst loading of the cathode was intentionally increased).

For the three $H_2$/Ar ratios, the high frequency limit of the impedance is real. The limit on the real axis is due to the series connection of the resistance of the measurement cell and the resistance of the solid polymer electrolyte. It is known from the PEM fuel cell literature [16] that the ionic resistance of Nafion membranes depends on the hydrogen partial pressure. In particular, is has been reported that a surface proton transfer mechanism along pore walls predominates at low pressure values and that the membrane resistivity decreases when $H_2$ partial pressure is lowered. However, this effect has been observed only for low $H_2$ partial pressures ($P_{H2} < 10$ kPa) while the partial pressure in the most diluted gas mixture used in this work is 30 kPa. This effect was not observed in our experiments (the high frequency resistance does not vary with $H_2$ partial pressure).

For pure $H_2$ ($P_{H2} = 100$ kPa) and for $H_2$/Ar = 1 ($P_{H2} = 50$ kPa), a characteristic 45° semi-line is observed in the high frequency range. The low frequency impedances are real and a significant increase of the overall cell impedance is observed as the hydrogen content of the

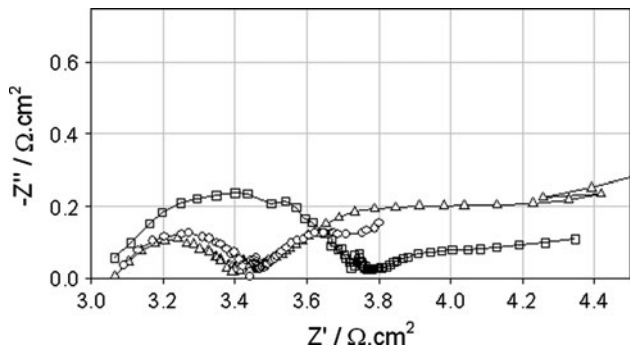


**Fig. 9** Impedance diagrams recorded under flooding conditions: $T_{hum} = 70$ °C and: (*square*) $E = 50$ mV; $T_{cell} = 43$ °C; (*circle*) $E = 50$ mV; $T_{cell} = 70$ °C; (*triangle*) $E = 100$ mV; $T_{cell} = 43$ °C

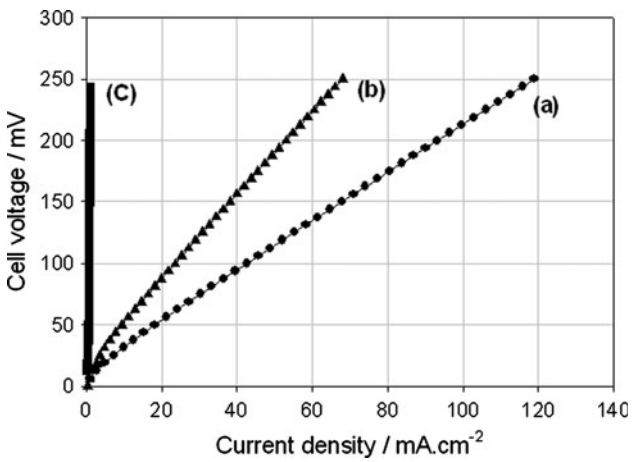


**Fig. 10** Polarisation curves measured at $T_{cell} = 60$ °C for three different $H_2$/Ar mole ratios. (*a*) pure $H_2$, (*b*) $H_2$/Ar = 1, (*c*) $H_2$/Ar = 0.3

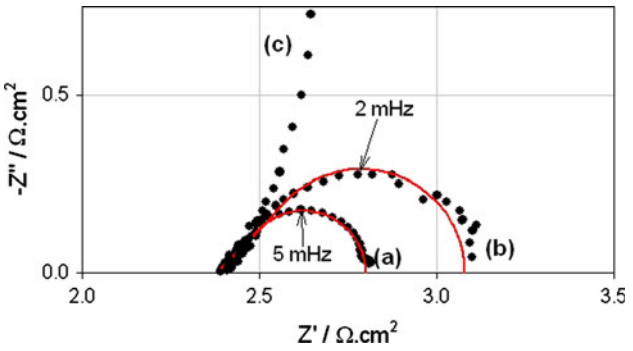


**Fig. 11** Impedance diagrams at $T_{cell} = 60$ °C and E = 0.1 V for different $H_2$/Ar mole ratios. (*dash*) best fit from Eq. 3. (*a*) pure $H_2$, (*b*) $H_2$/Ar = 1, (*c*) $H_2$/Ar = 0.3

hydrogen–argon gas mixture decreases. When hydrogen is strongly diluted (curve c), the 45° semi-line is also observed in the high frequency domain but over a limited range of frequencies. At low frequencies, there is a tendency to form a semi-circle as for less-diluted gas mixtures but the limit on the real axis is significantly larger (not shown in Fig. 11). This high frequency shape of the impedance diagrams suggest that diffusion-controlled mass-transport limitations are taking place. Such limitations can be due either to hydrogen diffusion in the gas phase to the electrode (gas convection due to the circulation of the gas mixture inside the cell is not expected to contribute to the efficient transport of hydrogen to the electrode in the vicinity of the reaction zone) or to hydrogen diffusion across a thin water film formed at the surface of catalysts particles (similar to flooding conditions). Both hypothesis (or a combination of the two) are consistent with the experimental observations. A simple model circuit can be used to fit experimental data. Assuming that the kinetics of the HER at the cathode is high, then the cell impedance ($Z_{cell}$) can be approximated by considering the series connection of (i) the sum of the cell ($R_{cell}$) and electrolyte ($R_{el}$) resistance; (ii) the impedance of the anode ($Z_a$). The impedance of the anode $Z_a$ is due to the parallel connection of the double layer capacitance ($C_{dl}$) and the charge transfer impedance. The charge transfer impedance is assumed to be limited by mass-transport limitations of $H_2$ to the anode ($Z_D$). According to the literature [17], the expression of $Z_D$ is given by Eq. 5:

$$Z_D\ (\omega) = R_D\,(\omega)\ \frac{\coth\ (\tau\ p)^{1/2}}{(\tau\ p)^{1/2}} \tag{5}$$

where $p = j\ \omega$ and j is the imaginary unit, $\tau = \delta^2/D$ is a time constant homogeneous to the second scale. $\delta$ (cm) is the thickness of the diffusion layer, D ($cm^2$ s) is the hydrogen diffusion coefficient in the feed gas mixture.

$R_D(\omega)$ is the diffusion resistance defined as:

$$R_D\,(\omega)\ = \frac{\delta}{F\ D\ \left(-\frac{\partial C}{\partial E}\right)} \tag{6}$$

$F$ is the faraday (96,490 C $mol^{-1}$); $\left(\frac{\partial C}{\partial E}\right)$ is the slope of the adsorption isotherm at the measurement point.

From the above-described model, the cell impedance $Z_{cell}$ is finally given by:

$$Z_{cell}\,(\omega) = \ (R_{cell} + R_{el})\ + \frac{1}{j\,C_{dl}\ \omega + \frac{1}{Z_D}} \tag{7}$$

Experimental impedance diagrams have been fitted using model Eq. 7. Results are plotted in Fig. 11. The characteristic pulsation $\omega_c$ (in rad $s^{-1}$) corresponding to the maximum value of the imaginary part of the impedance $\{-Z''\}$ and the characteristic frequency $f_c$ (in Hz) are related to the time constant of the mass-transport process [17]:

$$\omega_c = \ \frac{2.52}{\tau} = \frac{2.52\ D}{\delta^2} = 2\ \pi\ f_c \tag{8}$$

Best fit parameters of curves (a) and (b) (Fig. 3) with model Eq. 7 are compiled in Table 1.

Due to the structure of the anode (a powder of platinum particles is used as electrocatalyst and a PTFE-impregnated carbon cloth is used at gas diffusion layer), it is difficult to provide an estimation of the thickness $\delta$ of the diffusion layer. However, what can be determined from Fig. 11 is that, when the hydrogen content of the feed gas mixture decreases: (i) the diffusion impedance $R_D(\omega)$ increases; and (ii) the characteristic pulsation $\omega_c$ decreases. This is supporting the idea that hydrogen transport inside the gas phase plays a significant role in the overall kinetics. When the hydrogen concentration in the feed mixture is low (curve c in Fig. 11 where $H_2$/Ar = 0.3), then the diffusion impedance becomes very high. As a consequence, the possibility to extract hydrogen from a gas mixture using such electrochemical pump should be limited to sufficiently rich ($[H_2] > 50\%$) gas mixtures, in agreement with the results of Ref. [7]. The less concentrated the mixture is, the less efficient the process is.

**Table 1** Fit parameters of curves (a) and (b) of Fig. 3 using model Eq. 7

| | $R_{cell} + R_{el}$ ($\Omega$ $cm^2$) | $C_{dl}$ ($\mu$F $cm^{-2}$) | $R_D$ ($\Omega$ $cm^2$) | $\tau$ (s) | $f_c$ (Hz) |
|---|---|---|---|---|---|
| (a) Pure $H_2$ | 2.38 | 3.0 | 0.42 | 10.0 | $5.0 \times 10^{-3}$ |
| (b) $H_2$/Ar = 1.0 | 2.38 | 3.0 | 0.70 | 10.0 | $3.2 \times 10^{-3}$ |

## 4 Conclusions

The electrochemical performances of PEM membrane electrode assemblies used in hydrogen concentration cells have been analyzed using electrochemical impedance spectroscopy. Both cell conductivity and electrode activity have been measured. It is shown that the relative humidity of hydrogen plays a critical role. Best performances (lowest MEA resistances) were measured when the temperatures of the cell and gas humidifier were similar and close to 70 °C. Under such operating conditions, catalytic layers exhibited the highest activity. At lower temperatures, a larger membrane resistance and a lower activity of the catalyst layers were obtained. When the temperature difference between gas humidifier and measurement cell is too large (>10 °C), depletion of water required for membrane humidification is observed and the MEA resistance increases. It is also shown that the MEA resistance decreases when the ion-exchange polymer content in the cathode electrocatalytic layer is increased and when the humidifier temperature increases up to the cell temperature value. This is due to a better proton conductivity of the catalyst layer. Mass-transport limitations were observed in the gas phase when the hydrogen content in the gas mixture was decreased. It is shown that the use of such electrochemical pumps is limited to the treatment of gas mixtures in which the hydrogen content is sufficiently high (>50%).

**Acknowledgments** This work has been financially supported by the Ministry for Education and Science of the Russian Federation within the framework of the Federal Principal Scientific-Technical Programme "Researches and development on priority directions in development of scientific technological complex of Russia for 2007–2012" and by the ICTS (under contract no 00015.00010).

## References

1. Grigoriev SA, Shtatniy IG, Millet P, Porembsky VI, Fateev VN (2011) Description and characterization of an electrochemical hydrogen compressor/concentrator based on solid polymer electrolyte technology. Int J Hydrogen Energy 36(6):4148–4155
2. Gardner CL, Ternan M (2007) Electrochemical separation of hydrogen from reformate using PEM fuel cell technology. J Power Sources 171:835–841
3. Feindel KW, Bergens SH, Wasylishen RE (2007) Use of hydrogen–deuterium exchange for contrast in 1H NMR microscopy investigations of an operating PEM fuel cell. J Power Sources 173:86–95
4. Eichelhardt F, Cristescu I, Michling R, Welte S (2010) Modification of a solid polymer electrolyte (SPE) electrolyser to ensure tritium compatibility. Fusion Eng Design (in press)
5. Ibeh B, Gardner C, Ternan M (2007) Separation of hydrogen from a hydrogen/methane mixture using a PEM fuel cell. Int J Hydrogen Energy 32:908–914
6. Springer TE, Zavodzinski TA, Gottesfeld S (1991) Polymer electrolyte fuel cell model. J Electrochem Soc 138(8):2334–2342
7. Lee HK, Choi HY, Choi KH, Park JH, Lee TH (2004) Hydrogen separation using electrochemical method. J Power Sources 132: 92–98
8. Grigoriev SA, Millet P, Fateev VN (2008) Evaluation of carbon-supported Pt and Pd nanoparticles for the hydrogen evolution reaction in PEM water electrolysers. J Power Sources 177(2): 281–285
9. Grigoriev SA, Millet P, Volobuev SA, Fateev VN (2009) Optimization of porous current collectors for PEM water electrolysers. Int J Hydrogen Energy 34(11):4968–4973
10. Grigoriev SA, Millet P, Volobuev SA, Fateev VN (2009) Optimization of porous current collectors for PEM water electrolysers. Int J Hydrogen Energy 34:4968–4973
11. Saleh MM, Okajima T, Hayase M, Kitamura F, Ohsaka T (2007) Exploring the effects of symmetrical and asymmetrical relative humidity on the performance of H2/air PEM fuel cell at different temperatures. J Power Sources 164:503–509
12. Zhang J, Tang Y, Song C, Xia Z, Li H, Wang H, Zhang J (2008) PEM fuel cell relative humidity (RH) and its effect on performance at high temperatures. Electrochim Acta 53:5315–5321
13. Riascos LAM (2008) Relative humidity control in polymer electrolyte membrane fuel cells without extra humidification. J Power Sources 184:204–211
14. Barbir F (2005) PEM fuel cells, theory and practice. Academic Press, Elsevier, Burlington
15. Grigor'ev SA, Khaliullin MM, Kuleshov NV, Fateev VN (2001) Electrolysis of water in a system with a solid polymer electrolyte at elevated pressure. Russ J Electrochem 37(8):819–822
16. Vayenas CG, Tsampas MN, Katsaounis A (2007) First principles analytical prediction of the conductivity of Nafion membranes. Electrochim Acta 52:2244–2256
17. Barsoukov E, Macdonald JR (2005) Impedance spectroscopy, theory, experiment, and applications. Wiley, New York